Aquatic habits and niche partitioning in the extraordinarily long-necked Triassic reptile *Tanystropheus*

Stephan N. F. Spiekman,[1,8,*] James M. Neenan,[2] Nicholas C. Fraser,[3] Vincent Fernandez,[4,5] Olivier Rieppel,[6] Stefania Nosotti,[7] and Torsten M. Scheyer[1]

[1]Palaeontological Institute and Museum, University of Zurich, Karl-Schmid-Strasse 4, 8006 Zurich, Switzerland

[2]Oxford University Museum of Natural History, Parks Road, Oxford OX1 3PW, UK

[3]National Museums Scotland, Chambers St, Edinburgh EH1 1JF, UK

[4]European Synchrotron Radiation Facility, 71 Avenue des Martyrs, 38000 Grenoble, France

[5]The Natural History Museum, Cromwell Road, London SW7 5BD, UK

[6]Field Museum of Natural History, 1400 S Lake Shore Dr, Chicago, IL 60605, USA

[7]Museo Civico di Storia Naturale di Milano, Corso Venezia 55, 20121 Milan, Italy

[8]Lead Contact

*Corresponding author: stephanspiekman@gmail.com

Summary

***Tanystropheus longobardicus* is one of the most remarkable and iconic Triassic reptiles. Mainly known from the Middle Triassic conservation Lagerstätte of Monte San Giorgio on the Swiss-Italian border, it is characterized by an extraordinarily long and stiffened neck that is almost three times the length of the trunk, despite being comprised of only 13 hyper-elongate cervical vertebrae [1-8]. Its palaeobiology remains contentious, with both aquatic and terrestrial lifestyles having been proposed [1, 9-12]. Among the *Tanystropheus* specimens, a small morphotype bearing tricuspid teeth and a large morphotype bearing single-cusped teeth can be recognized, historically considered as juveniles and adults of the same species [4]. Using high-resolution synchrotron radiation microtomography (SRμCT), we three-dimensionally reconstruct a virtually complete but disarticulated skull of the large morphotype, including its endocast and inner ear, to reveal its morphology for the first time. The skull is specialized towards hunting in an aquatic environment, indicated by the placement of the nares on the top of the snout and a 'fish-trap' type dentition. The SRμCT data and limb bone palaeohistology reveal that the large morphotype represents a separate species (*Tanystropheus hydroides* sp. nov.). Skeletochronology of the small morphotype specimens indicates that they are skeletally mature despite their small size, thus representing adult individuals of *Tanystropheus longobardicus*. The co-occurrence of these two species of disparate size ranges and dentitions provides strong evidence for niche partitioning, highlighting the surprising versatility of the *Tanystropheus* bauplan and the complexity of Middle Triassic nearshore ecosystems.**

Keywords: Aquatic adaptations, Niche partitioning, Triassic, Archosauromorpha, Synchrotron Microtomography, Bone histology

Results

Systematic palaeontology

Diapsida Osborn, 1903 [13]

Archosauromorpha von Huene, 1946 [14]

Tanystropheidae Camp 1945 [15]

Tanystropheus von Meyer, 1852 [16]

Tanystropheus hydroides sp. nov.

Etymology

'Hydra' refers to the long-necked mythical sea monster of Greek antiquity; the suffix *-oides* means 'related to' or 'resembling' in Ancient Greek. The name refers to the resemblance of *T. hydroides* to this famous mythological creature.

Holotype

PIMUZ T 2790, a semi-articulated specimen consisting of a virtually complete yet strongly compressed skull and the first eight cervical vertebrae.

Referred material

PIMUZ T 2787, PIMUZ T 2793, PIMUZ T 2818, PIMUZ T 2819, PIMUZ T 183, SNSB-BSPG 1953 XV 2, MSNM V 3663. A synonymy list is provided in ref. [17] (as the large morphotype of *T. longobardicus*).

Locality

Monte San Giorgio on the border of Switzerland (canton Ticino) and Italy (Lombardy).

Horizon

Besano Formation, Anisian-Ladinian boundary, Middle Triassic.

Diagnosis

The recently revised generic diagnosis for *Tanystropheus* remains valid [17]. The following diagnosis distinguishes *Tanystropheus hydroides* from other *Tanystropheus* species (autapomorphies among Triassic archosauromorphs indicated by an asterisk): premaxilla lacking a postnarial process; single cusped marginal dentition; dentary tooth piercing through a foramen in the maxilla*; depression on the dorsal surface of the nasals; straight suture between frontals; fused parietal; conspicuously hooked dorsal quadrate head; wide and anteriorly rounded vomers with a single row of large recurved teeth along its outer margin*; edentulous palatine and pterygoid; dentary bearing a distinct ventral keel at its anterior end*; a maximum total length of over 5 metres.

Cranial Description of **Tanystropheus hydroides**

The fossilised skull of PIMUZ T 2790 is heavily compressed, obscuring much of its anatomy (Figure 1A). However, the compression caused individual bones to disarticulate rather than deform, so they

largely maintain their three-dimensional morphology. Furthermore, the dorsal part of the skull has been displaced posteriorly, essentially folding over the rest of the skull bones. Consequently, many of the bones of the posterior part of the skull are well-preserved underneath the large frontals, which cover them. The digital models rendered from the SRμCT dataset allow the elements to be placed into their *in-vivo* position, thus 're-assembling' the skull (Figures 1G and 2). The skull is virtually complete and only parts of the nasal and anterior palatal elements are missing. For some paired bones, only a single element was well-preserved, in which case a copied and mirrored version of the best represented or only available element was added to the digital model in Blender (see Table S1).

The digital model of PIMUZ T 2790, supplemented by information from other specimens, allows for the detailed reconstruction of the skull of *T. hydroides* (Figure 3A-C), which strongly deviates from the previous reconstruction of the large morphotype of *T. longobardicus* [4].

The premaxilla is dorsoventrally tall and lacks both prenarial and postnarial processes that are common in early archosauromorphs and of which the latter is well-developed in *T. longobardicus* (Figures 2 and 3) [1, 18]. It bears six long curved fangs, of which the anterior three are the largest and interlocked with the corresponding fangs of the dentary to form a 'fish-trap' dentition, similar to that described for Triassic sauropterygian predators such as *Nothosaurus jagisteus* (SMNS 56618) and *Yunguisaurus liae* (NMNS 004529/F003862) [19, 20]. The maxillary teeth are smaller and peg-like; they are largest at mid-length of the maxilla and gradually reduce in size towards the anterior and posterior ends of the bone. Marginal dentition was subthecodont, with all teeth lacking serrations but bearing clear proximodistal striations. The 10th dentary tooth pierced through the maxilla above. This can be observed on both sides of PIMUZ T 2790, and a similar opening is also present in the right maxilla of *T. hydroides* specimen PIMUZ T 2819 (Figure S1A-B). The maxilla curves strongly medially at its dorsal margin, indicating that the nasals were entirely dorsal facing and only minimally visible in lateral view.

Only fragments of the nasals are preserved in PIMUZ T 2790, but they bear a clear concavity, which can also be seen on the fragmentary nasal remains of PIMUZ T 2819 (Figure S1A-B, see also figure 3 of ref. [21]). This concavity resembles the narial recess of the closely related, aquatic archosauromorph *Dinocephalosaurus orientalis* (IVPP V13767) [22]. The outline of the nasal and its articulation with the frontal can be inferred from the *T. hydroides* specimen PIMUZ T 2787 (Figure S2B), which reveals that the nasals were broad, plate-like elements, with an anterolateral process but lacking an anteromedial process. The absence of the anteromedial process of the nasal and the prenarial process of the premaxilla implies that an internarial bar was absent and that the external nares were confluent. As such, the overall construction of the snout and external nares is reminiscent of that of crown-group crocodylians, in particular that of *Purussaurus* spp. (Figure 3B) [23].

The frontals are unfused and very broad, largely flattened elements. As such, they formed a wide surface of the skull roof above the orbits, which were largely laterally facing (Figures 2-3B). The lateral margin of each frontal is slightly curved and forms the dorsal rim of each orbit.

The configuration of the temporal region of *Tanystropheus* differs strongly from that of other early archosauromorphs. The supratemporal fenestrae are entirely dorsally facing, and the intertemporal bar is formed jointly by a dorsoventrally tall postorbital and squamosal (Figure 1F). The fused parietal possesses pronounced anterolateral and posterolateral processes and bears deep, largely laterally facing, supratemporal fossae (Figure 3B). The squamosal bears a peculiar socket for the reception of

the quadrate on its posteroventral surface (Figure 1E). This socket is profoundly deep and was likely covered by a cartilaginous cap. The dorsal head of the quadrate is extended posteriorly to form a posteroventrally directed hook (Figure 1F), similar to that described for the allokotosaur *Azendohsaurus madagaskarensis* (FMNH PR 2751) [24]. The posteriorly enlarged articulation surface on the dorsal head of the quadrate and the deep socket on the squamosal allowed for an anteroposteriorly sliding contact between them. This indicates the presence of streptostyly, or the ability of the quadrate to move independently of other cranial bones [25], which has previously been tentatively suggested for *Tanystropheus* [4]. A quadratojugal is identified confidently for the first time in *Tanystropheus*. It is a small and curved, rod-like bone (Figures 1F, 2-3). Ventrally it connects to a facet on the lateroventral condyle of the quadrate and connects to the quadrate and squamosal on its dorsal end. As such it does not contact the posterior process of the jugal and thus the infratemporal bar is incomplete.

The palatal elements almost completely enclosed the palatal surface, similar to *D. orientalis* (IVPP V13898) [22]. The internal choanae were narrow, as indicated by the wide and plate-like vomers. The vomer has a continuously curved outer margin, along which a single row of 15 enlarged recurved teeth is arranged (Figure S2A). The anterior rami of the pterygoids are poorly preserved in PIMUZ T 2790, but their shape can be inferred from PIMUZ T 2787, which reveals that they were wide and anteriorly rounded (Figure S2C). Both the pterygoid and palatine are edentulous. This is in stark contrast to *T. longobardicus*, in which the shape of the vomer, palatine, and pterygoid is distinctly different and all these elements are tooth-bearing (Figure 3F) [17]. The ectopterygoid identified in PIMUZ T 2790 differs strongly in shape from former interpretations, as this element was probably misidentified previously (Figures 2D and 3C) [4].

The SRµCT data also allows for the first detailed observation of the braincase of *Tanystropheus* and reveals the presence of a small laterosphenoid that dorsally encloses the opening for cranial nerve V (Figure S1C). This represents the most stem-ward known occurrence of a laterosphenoid in the archosaur lineage [26-28]. The excellent preservation of the braincase also allowed for the partial reconstruction of the endocast and endosseous labyrinth (Figure 1D). The flocculus, part of the cerebellum, forms a laterally protruding, bulbous lobe in *T. hydroides*. The endosseous labyrinth is complete except for the anterior semicircular canal. However, its shape can be roughly inferred from the shape of the flocculus, over which this canal would have curved.

The dentary bears a distinct ventral keel at its anterior end, which is absent in *T. longobardicus* (Figures 2A-B and 3). The posterior margin of the glenoid fossa forms a short vertical bony protrusion that would have prevented the quadrate from dislocating from the mandible during retraction. The articular forms a distinct but not upturned retroarticular process.

Discussion

The lifestyle of T. hydroides *and* T. longobardicus

Inferences for the diet of *T. hydroides* can be made based on stomach contents that have been identified in at least two different specimens. In PIMUZ T 2793 a large number of belemnoid cephalopod hooklets are scattered in the area between the articulated gastralia and in PIMUZ T 2817 a large accumulation of ganoid fish scales is present in the stomach region [4]. The new skull reconstruction adds crucial information vital to confidently assess the palaeobiology and feeding mechanism of *T. hydroides*. Suction feeding can be excluded, since the lower jaws are tightly

connected at the symphysis and would not have allowed the required expansion of the buccal cavity and because the hyoid apparatus lacks an ossified hyoid corpus or robust hyobranchial elements present in suction-feeding amniotes [4, 29, 30]. Furthermore, the large fang-like anterior teeth of *T. hydroides* would interfere with the prey item entering the buccal cavity during suction feeding. The most likely feeding strategy for *T. hydroides* is that of a 'ram-feeder' (sensu ref. [30]). By employing a laterally directed snapping bite, a prey item would be secured by the procumbent fang-like marginal teeth, aided by the second row of sharp teeth on the outer margin of the vomers. The flattened shape of the snout and the placement of the external nares on its dorsal surface support an at least semi-aquatic lifestyle for *T. hydroides* and would have reduced drag when the head was moved laterally (Figures 2 and 3A).

The poor hydrodynamic profile and limited appendicular adaptations to an aquatic lifestyle indicate that both *T. hydroides* and *T. longobardicus* were neither fast nor efficient swimmers (Figure 3G) [1, 31], unlike the closely related *D. orientalis* [22, 32]. Furthermore, the elongate and gracile semicircular canals of the endosseous labyrinth of *T. hydroides* reveal that it did not have a pelagic or deep-diving lifestyle (Figure 1D) [33-36]. This indicates that *T. hydroides* was likely restricted to coastal and possibly freshwater environments, which is supported by the occurrence of *Tanystropheus*-like cervical vertebrae in fluvial deposits in North America [37]. It is highly unlikely that *T. hydroides* was able to catch fast moving prey such as actinopterygian fishes and belemnoid cephalopods through active pursuit. Rather it seems that *T. hydroides* was an ambush predator. The head is particularly small given the overall size of the animal and is positioned on an extraordinarily long and slender neck. Therefore, *T. hydroides* might have been able to approach its prey whilst being positioned on the sea floor or let its prey approach it without triggering a flight response, especially in turbid water, as has also been hypothesised for certain long-necked plesiosaurs [31, 38].

Niche partitioning in a highly specialized reptile

LAGs are periodically formed when bone growth is drastically slowed down during cyclical annual events that reduce metabolism and energy intake (e.g. cold seasons or dry periods), and therefore can be used to approximate the age of an individual [39, 40]. When LAGs occur in close succession at the outer margin of the cortex (i.e. OCL), this implies that growth in the individual had drastically decreased, indicating skeletal maturity. The combined presence of a large number of LAGs and an OCL in the limb elements of the small morphotype specimen PIMUZ T 1277 is a clear indication that this individual was skeletally mature when it died (Figure 4A, C-D) [41]. The total body length of PIMUZ T 1277 is approximately 1.5 metres [5], whereas the largest known specimen of *T. hydroides* is more than 3.5 times longer (Figure 3G) [4]. From this large size discrepancy, it can unequivocally be determined that the specimens bearing tricuspid teeth represent a small species distinct from *T. hydroides*. Together with their distinctly different dentitions (Figure 3A-F), this implies that *T. hydroides* and *T. longobardicus* certainly exploited different food sources. The tricuspid dentition seen in *T. longobardicus* has a broad utilization among extant squamates and is widespread among insectivores and omnivores [42]. Therefore, a possible broad diet comprised of small animals including soft-shelled invertebrates such as decapod crustaceans is here proposed for *T. longobardicus*.

Both *T. hydroides* and *T. longobardicus* are known from several articulated and disarticulated specimens from the Besano Formation of Monte San Giorgio. Although it cannot be excluded that the carcasses of these taxa were transported to their bedding position after death, both species

show a similar taphonomic pattern [9], and it is most likely that both taxa co-occurred in the same habitat. The clear distinction in feeding strategy thus presents a strong indication of niche partitioning between these two species. Niche partitioning has previously been reported for Mesozoic marine reptiles [43, 44], and was tentatively suggested for *Tanystropheus* material from the Middle Triassic Maktesh Ramon locality of Israel [17, 45]. Niche partitioning has also been invoked for the actinopterygian *Saurichthys* [8, 46, 47] and amongst perleidid fishes [48] from the Middle Triassic of Monte San Giorgio. Indeed, habitat partitioning appears to be a repeated pattern in Triassic marine basin biota. It is remarkable that such a striking partitioning occurred comparatively soon after the End-Permian mass extinction in a highly specialized genus. Previously it was considered that the neck of *Tanystropheus* formed a morphological constraint and severely limited its ecological adaptability [49, 50]. Our findings reveal that the neck of *Tanystropheus* was more multifunctional than previously considered and allowed the exploitation of various food sources. Furthermore, the wide distribution of specimens that are morphologically indistinguishable from *T. hydroides* across the Tethys basin highlights the efficiency of the *Tanystropheus* bauplan [6, 17].

Conclusions

Reconstructing the morphology and palaeobiology of long extinct organisms without close modern analogues is crucial in our understanding of biological diversity through time and approximating the ecomorphological limitations of life. The bizarre *Tanystropheus* represents a particularly interesting case study in this regard due to its unique morphology among tetrapods, exemplified by its extremely long neck consisting of only 13 very elongate vertebrae. The skull of PIMUZ T 2790 reveals that the cranial morphology of *T. hydroides* deviated strongly from that of other early archosauromorphs. The cranial reconstruction indicates that *T. hydroides* hunted in an aquatic environment, using its long fang-like teeth and a lateral snapping bite to seize its prey. *Tanystropheus hydroides* and *T. longobardicus* were two closely related species that almost certainly co-occurred in the same habitat. This remarkable case of niche partitioning highlights the versatility of the *Tanystropheus* bauplan and the complexity of Middle Triassic marine trophic networks, within 10 million years after the End-Permian extinction event, and the major role of reptiles therein.

Acknowledgements

We are very thankful for the full-body skeletal reconstructions of the two *Tanystropheus* species by Beat Scheffold (PIMUZ). Christian Klug (PIMUZ) is thanked for specimen access and allowing us to remove the skull of PIMUZ T 2790 from the larger slab. Dylan Bastiaans, Feiko Miedema, Christian Klug, Roger Benson, Erin Saupe, Jonah Choiniere, Roland Sookias, Richard Butler, Fabio Dalla Vecchia, Pernille Troelsen, Oliver Rauhut, Gabriela Sobral, and Dennis Voeten are thanked for fruitful discussions. We thank the European Synchrotron Radiation Facility (ESRF), Grenoble, France, for provision of synchrotron radiation beamtime at beamline BM05. This study is part of the SNSF project granted to TMS (grant no. 2'5321-162775). JMN was funded by a Leverhulme Trust Early Career Fellowship (ECF-2017-360). We kindly thank editor Florian Maderspacher and two anonymous reviewers for their helpful suggestions that improved the quality of this manuscript.

Author Contributions

SNFS, TMS, NCF, OR, and SN designed the study. VF and SNFS performed the synchrotron scanning and processed the data. SNFS segmented the skull. JMN and SNFS segmented the endocast and

endosseous labyrinth. TMS and SNFS made the histological sections. SNFS performed the phylogenetic analysis. SNFS and TMS made the figures. SNFS, TMS, and VF wrote the manuscript. All authors reviewed a final draft of the manuscript.

Declaration of Interests

The authors declare no competing interests.

Main Figure Titles and Legends

Figure 1. The skull of *Tanystropheus hydroides* sp. nov. holotype PIMUZ T 2790. (A) The complete skull in dorsal view. (B) Digital rendering of the skull in dorsal view, (C) and ventral view. This model is also presented in Video S1. (D) Digital rendering of the endocast and endosseous labyrinth (mirrored). (E) Digital rendering of the right squamosal in posterolateral view. (F) Reconstruction of the temporal region in oblique right lateral view, highlighting the streptostylic articulation of the quadrate and squamosal. (G) The digitally 're-assembled' skull of PIMUZ T 2790 in angled left lateral view. This model is also presented in Video S2. Bone colour codings can be found in Table S1. Abbreviations: CN, cranial nerve.

Figure 2. The complete 're-assembled' digital model of PIMUZ T 2790. (A) Right lateral, (B) left lateral, (C) occipital, (D) ventral, and (E) dorsal view. This model is also presented in Video S2. Bone colour codings can be found in Table S1.

Figure 3. Interpretative reconstruction drawings of *Tanystropheus hydroides* sp. nov. and *Tanystropheus longobardicus*. Reconstruction drawings of the skull and mandible of *Tanystropheus hydroides* sp. nov. in (A) left lateral, (B) dorsal, and (C) ventral view, and *Tanystropheus longobardicus* in (D) left lateral, (E) dorsal, and (F) ventral view. A revision of the cranial morphology of *Tanystropheus longobardicus* is provided in Methods S1. Important morphological details from *Tanystropheus* specimens other than the SRµCT scanned PIMUZ T 2790 can be found in Figures S1 and S2, in addition to a digital rendering of the right braincase showing the laterosphenoid in PIMUZ T 2790. (G) Complete skeletal reconstructions of *Tanystropheus hydroides* and *Tanystropheus longobardicus* with the outline of a 170 cm tall human in scuba diving equipment for scale. Abbreviations: **an**, angular; **ar**, articular; **bo**, basioccipital; **de**, dentary; **ect**, ectopterygoid; **fr**, frontal; **j**, jugal; **la**, lacrimal; **mx**, maxilla; **na**, nasal; **pa**, parietal; **pal**, palatine; **pbs**, parabasisphenoid; **pmx**, premaxilla; **po**, postorbital; **pof**, postfrontal; **pra**, prearticular; **prf**, prefrontal; **pt**, pterygoid; **q**, quadrate; **qj**, quadratojugal; **sq**, squamosal; **vo**, vomer.

Figure 4. Palaeohistological sections of *Tanystropheus longobardicus*. (A) Close-up of the cortex of the femur of PIMUZ T 1277 in normal transmitted light. (B) Close-up of the cortex of the femur of PIMUZ T 2484 in normal transmitted light. (C, D) Overview of complete cross-section and close-up of the cortex of the zeugopodial element of PIMUZ T 1277. Image (C) in normal transmitted light; image (D) in cross-polarised light using lambda compensator. Small arrow heads in (A) indicate growth marks within the cortical outer circumferential layer, whereas larger arrow heads generally indicate LAGs in the deeper parts of the cortex. Abbreviations: **LZB**, lamellar-zonal bone; **ocl**, outer circumferential layer (= external fundamental system); **rc**, radial vascular canals. All histological samples are presented in Figure S3 and described in Methods S1.

STAR Methods

Resource Availability

Lead contact

Further information and requests for resources and reagents should be directed to and will be fulfilled by the Lead Contact, Stephan N.F. Spiekman (stephanspiekman@gmail.com).

Material availability

This study did not generate new unique reagents.

Data availability

The digital models and SRµCT data of PIMUZ T 2790 can be found at https://www.paleo.esrf.fr. All histological slides used in the study are provided in Figure S3.

Institutional repositories

Bayerische Staatssammlung für Paläontologie und Geologie, Munich, Germany (BSPG); Field Museum of Natural History, Chicago, USA (FMNH); Institute of Vertebrate Paleontology and Paleoanthropology, Beijing, China (IVPP); Museo di Storia Naturale, Milan, Italy (MSNM); National Museum of Natural Science, Taichung City, Taiwan (NMNS); Paläontologisches Institut und Museum der Universität Zürich, Zurich, Switzerland (PIMUZ); Staatliches Museum für Naturkunde, Stuttgart, Germany (SMNS).

Experimental Model and Subject Details

The experimental subjects of this study comprise several fossil specimens belonging to the tanystropheid archosauromorph genus *Tanystropheus*, most notably PIMUZ T 2790, which was subjected to SRµCT scanning. *Tanystropheus longobardicus* specimens PIMUZ T 2484 and PIMUZ T 1277 were sectioned for bone histology. The cranial reconstructions of both *Tanystropheus* species were made based on morphological observations made from PIMUZ T 2790, PIMUZ T 2819, PIMUZ T 2787, and PIMUZ T 2484. All specimens and histological slides are reposited at the Palaeontological Institute and Museum of the University of Zurich, Switzerland (PIMUZ).

Method details

Synchrotron micro Computer Tomography acquisition and image processing

The specimen was scanned at the BM05 beamline of the European Synchrotron Radiation Facility (ESRF, Grenoble, France) using propagation phase contrast synchrotron radiation micro-computed tomography. The experimental setup consisted of: filtered white beam (bending magnet, filters: 18 rods of Al, 5 mm in diameter and 10 cm in length, Mo 0.25 mm) with a total integrated detected energy of 115 keV, a sample-detector propagation distance of 4 m and an indirect detector (2 mm LuAG scintillator 0.25x magnification, CCD FReLoN 2K camera) producing data with a measured isotropic voxel size of 46.76 µm. To image the full sample, the centre or rotation was shifted to increase the lateral field of view by ~30%, and 77 acquisitions were necessary on the vertical axis (keeping a 50% overlap between consecutive scans). Each acquisition consisted of 2999 projections of a total integration time of 0.3 seconds (10 frames of 0.03 second per projection in accumulation mode [51]) over a rotation of 360°. Tomographic reconstruction was achieved with PyHST2 [52], using the single distance phase retrieval approach [53]. Post processing included: modification of the

bit depth from 32 bits to 16 bits as a stack of tiff, merging of the 77 datasets using a weighted average on overlapping parts, ring correction [54]; cropping of the volume.

The data was segmented and reconstructed in Mimics Research v19.0 (https://biomedical.materialise.com/mimics; Materialise NV, Leuven, Belgium). The models of the individual elements were imported as PLY files into Blender 2.7 (https://blender.org; Stitching Blender Foundation, Amsterdam, the Netherlands), a 3D modelling and visualisation program in which the elements could be rotated and moved independently, and images could be rendered, applying colours and texture to the models. As an aid to establish bone contacts, most elements were printed using a MakerBot Replicator 2X 3D printer (https://makerbot.com; MakerBot Industries, LLC, New York City, USA). This way, using both the digital and printed models, the connections between the bones could be restored in high detail, allowing for the confident reconstruction of the skull.

Bone histology

Three bones of two separate specimens of *T. longobardicus* were sampled for analysis of bone histology. From PIMUZ T 1277 we sampled a femur and a zeugopodial element and from PIMUZ T 2484, we sampled a femur. Thin slices of the bones were removed from the slabs using a small diamond-studded saw blade on a Dremel drill. The samples were then embedded in synthetic resin and ground down to about 60-100 microns thick slides using SIC powders (220, 500 and 800), following standard protocols [55]. The thin-sections were studied and photographed using a LEICA compound microscope DM 2500 M equipped with digital camera DFC 420C (an overview of the slides can be found in Figure S3).

Quantification and Statistical Analysis

Phylogenetic analysis

The interrelationships of tanystropheid archosauromorphs have previously been tested with a dedicated character matrix [56], which has subsequently been modified and expanded upon in order to investigate broader archosauromorph and early diapsid phylogeny [57-59]. We modified the most recent iteration of this matrix [60] in order to evaluate the implications of our findings for tanystropheid and early archosauromorph phylogeny. *Colobops noviportensis* is known from a single skull of a likely very early juvenile individual. Although recovered as an early diverging rhynchosaur in ref. [60], a recent re-analysis of this taxon has revealed it is actually a rhynchocephalian lepidosauromorph [61]. The inclusion of a poorly known rhynchocephalian based on an ontogenetically early specimen is not beneficial in resolving early archosauromorph phylogeny and might introduce unnecessary biases, and therefore *C. noviportensis* was excluded here. *Boreopricea funerea* is also known from a single specimen that is poorly preserved and several elements of this specimen have likely been misplaced, which introduces the possibility of unreliable character observation [18, 62], and it was therefore also excluded. The modifications made to the characters and the updated data matrix can be found in Methods S1. We analysed the matrix according to the maximum parsimony criterion in TNT 1.5 [63], using the Traditional Search algorithm. The same parameters described in ref. [60] were used to analyse the data and calculate the support values, in order to directly compare results. Three most parsimonious trees with 1125 steps were recovered (CI=0.324; RI=0.648) (the complete strict consensus tree, including Bootstrap and Bremer support values, can be found in Figure S4).

Methods S1. Revision of *Tanystropheus longobardicus*, related to Figure 3D-F. Description of histological sections, related to Figure 4. Results and discussion of phylogenetic analysis, related to STAR Methods.

Multimedia Files

Video S1. Rotating video of the in-situ model of the skull of PIMUZ T 2790. Related to Figure 1.

Video S2. Rotating video of the 're-assembled' model of the skull of PIMUZ T 2790. Related to Figures 1 and 2.

Data S1. Nexus file with the modified character matrix of Pritchard et al. (2018) [S23]. Related to STAR Methods.

References

1. Nosotti, S. (2007). *Tanystropheus longobardicus* (Reptilia, Protorosauria): Re-interpretations of the anatomy based on new specimens from the Middle Triassic of Besano (Lombardy, northern Italy). Memorie della Società Italiana di Scienze Naturali e del Museo Civico di Storia Naturale di Milano *35*, 1-88.
2. Peyer, B. (1931). Die Triasfauna der Tessiner Kalkalpen II. *Tanystropheus longobardicus* Bass. sp. Abhandlungen der Schweizerischen Paläontologischen Gesellschaft *50*, 9-110.
3. Tschanz, K. (1986). Funktionelle Anatomie der Halswirbelsäule von *Tanystropheus longobardicus* (Bassani) aus der Trias (Anis/Ladin) des Monte San Giorgio (Tessin) auf der Basis vergleichend morphologischer Untersuchungen an der Halsmuskulatur rezenter Echsen. PhD thesis Universität Zürich.
4. Wild, R. (1973). Die Triasfauna der Tessiner Kalkalpen XXII. *Tanystropheus longobardicus* (Bassani) (Neue Ergebnisse). Schweizerische Paläontologische Abhandlungen *95*, 1-182.
5. Wild, R. (1980). Neue Funde von *Tanystropheus* (Reptilia, Squamata). Schweizerische Palaontologische Abhandlungen *102*.
6. Rieppel, O., Jiang, D.-Y., Fraser, N.C., Hao, W.-C., Motani, R., Sun, Y.-L., and Sun, Z.-Y. (2010). *Tanystropheus* cf. *T. longobardicus* from the early Late Triassic of Guizhou Province, southwestern China. Journal of Vertebrate Paleontology *30*, 1082-1089.
7. Taylor, M.P., and Wedel, M.J. (2013). Why sauropods had long necks; and why giraffes have short necks. PeerJ *1*, e36.
8. Stockar, R. (2010). Facies, depositional environment, and palaeoecology of the Middle Triassic Cassina beds (Meride Limestone, Monte San Giorgio, Switzerland). Swiss Journal of Geosciences *103*, 101-119.
9. Beardmore, S.R., and Furrer, H. (2017). Land or water: using taphonomic models to determine the lifestyle of the Triassic protorosaur *Tanystropheus* (Diapsida, Archosauromorpha). Palaeobiodiversity and Palaeoenvironments *98*.
10. Jaquier, V.P., and Scheyer, T.M. (2017). Bone Histology of the Middle Triassic Long-Necked Reptiles *Tanystropheus* and *Macrocnemus* (Archosauromorpha, Protorosauria). Journal of Vertebrate Paleontology.
11. Renesto, S. (2005). A new specimen of *Tanystropheus* (Reptilia Protorosauria) from the Middle Triassic of Switzerland and the ecology of the genus. Rivista Italiana di Paleontologia e Stratigrafia *111*, 377-394.
12. Renesto, S., and Saller, F. (2018). Evidences for a semi aquatic life style in the Triassic diapsid reptile *Tanystropheus*. Rivista Italiana di Paleontologia e Stratigrafia *124*, 23-34.

13. Osborn, H.F. (1903). The reptilian subclasses Diapsida and Synapsida and the early history of the Diaptosauria. Memoirs of the American Museum of Natural History *1*, 449-519.
14. Huene, F.R.v. (1946). Die grossen Stämme der Tetrapoden in den geologischen Zeiten. Biologisches Zentralblatt *65*, 268-275.
15. Camp, C.L. (1945). *Prolacerta* and the protorosaurian reptiles. Part I and Part II. American Journal of Science *243*, 17-32, 84-101.
16. Meyer, H.v. (1855). Die Saurier des Muschelkalkes mit Rücksicht auf die Saurier aus buntem Sandstein und Keuper. In Zur Fauna der Vorwelt, zweite Abtheilung, H. Keller, ed. (Frankfurt a.m.: Heinrich Keller).
17. Spiekman, S.N.F., and Scheyer, T.M. (2019). A taxonomic revision of the genus *Tanystropheus* (Archosauromorpha, Tanystropheidae). Palaeontologia Electronica *22*, 1-46.
18. Ezcurra, M.D. (2016). The phylogenetic relationships of basal archosauromorphs, with an emphasis on the systematics of proterosuchian archosauriforms. PeerJ *4*, e1778.
19. Rieppel, O. (2002). Feeding mechanics in Triassic stem-group sauropterygians: the anatomy of a successful invasion of Mesozoic seas. Zoological Journal of the Linnean Society *135*, 33-63.
20. Cheng, Y.-N., Sato, T., Wu, X.-C., and Li, C. (2006). First complete pistosauroid from the Triassic of China. Journal of Vertebrate Paleontology *26*, 501-504.
21. Jiang, D.-Y., Rieppel, O., Fraser, N.C., Motani, R., Hao, W.-C., Tintori, A., Sun, Y.-L., and Sun, Z.-Y. (2011). New information on the protorosaurian reptile *Macrocnemus fuyuanensis* Li et al., 2007, from the Middle/Upper Triassic of Yunnan, China. Journal of Vertebrate Paleontology *31*, 1230-1237.
22. Rieppel, O., Li, C., and Fraser, N.C. (2008). The skeletal anatomy of the Triassic protorosaur *Dinocephalosaurus orientalis*, from the Middle Triassic of Guizhou Province, southern China. Journal of Vertebrate Paleontology *28*, 95-110.
23. Aguilera, O.A., Riff, D., and Bocquentin-Villanueva, J. (2006). A new giant *Purussaurus* (Crocodyliformes, Alligatoridae) from the upper Miocene Urumaco formation, Venezuela. Journal of Systematic Palaeontology *4*, 221-232.
24. Flynn, J.J., Nesbitt, S.J., Michael Parrish, J., Ranivoharimanana, L., and Wyss, A.R. (2010). A new species of *Azendohsaurus* (Diapsida: Archosauromorpha) from the Triassic Isalo Group of southwestern Madagascar: cranium and mandible. Palaeontology *53*, 669-688.
25. Smith, K.K. (1980). Mechanical significance of streptostyly in lizards. Nature *283*, 778-779.
26. Clark, J.M., Welman, J., Gauthier, J.A., and Parrish, J.M. (1993). The laterosphenoid bone of early archosauriforms. Journal of Vertebrate Paleontology *13*, 48-57.
27. Sobral, G., and Müller, J. (2019). The braincase of *Mesosuchus browni* (Reptilia, Archosauromorpha) with information on the inner ear and description of a pneumatic sinus. PeerJ *7*, e6798.
28. Sobral, G., Sookias, R.B., Bhullar, B.-A.S., Smith, R.M.H., Butler, R.J., and Müller, J. (2016). New information on the braincase and inner ear of *Euparkeria capensis* Broom: implications for diapsid and archosaur evolution. Royal Society Open Science *3*.
29. Lauder, G. (1985). Aquatic feeding in lower vertebrates. In Functional vertebrate morphology, M. Hildebrand, D. Bramble, K. Liem and D. Wake, eds. (Cambridge: Harvard University Press), pp. 210-229.
30. Motani, R., Ji, C., Tomita, T., Kelley, N., Maxwell, E., Jiang, D.-y., and Sander, P.M. (2013). Absence of suction feeding ichthyosaurs and its implications for Triassic mesopelagic paleoecology. PLoS One *8*.
31. Massare, J.A. (1988). Swimming capabilities of Mesozoic marine reptiles: implications for method of predation. Paleobiology *14*, 187-205.
32. Liu, J., Organ, C.L., Benton, M.J., Brandley, M.C., and Aitchison, J.C. (2017). Live birth in an archosauromorph reptile. Nature communications *8*, 14445.
33. Evers, S.W., Neenan, J.M., Ferreira, G.S., Werneburg, I., Barrett, P.M., and Benson, R.B. (2019). Neurovascular anatomy of the protostegid turtle *Rhinochelys pulchriceps* and

comparisons of membranous and endosseous labyrinth shape in an extant turtle. Zoological Journal of the Linnean Society *187*, 800-828.
34. Neenan, J.M., Reich, T., Evers, S.W., Druckenmiller, P.S., Voeten, D.F., Choiniere, J.N., Barrett, P.M., Pierce, S.E., and Benson, R.B. (2017). Evolution of the sauropterygian labyrinth with increasingly pelagic lifestyles. Current Biology *27*, 3852-3858. e3853.
35. Neenan, J.M., and Scheyer, T.M. (2012). The braincase and inner ear of *Placodus gigas* (Sauropterygia, Placodontia)—a new reconstruction based on micro-computed tomographic data. Journal of Vertebrate Paleontology *32*, 1350-1357.
36. Schwab, J.A., Young, M.T., Neenan, J.M., Walsh, S.A., Witmer, L.M., Herrera, Y., Allain, R., Brochu, C.A., Choiniere, J.N., and Clark, J.M. (2020). Inner ear sensory system changes as extinct crocodylomorphs transitioned from land to water. Proceedings of the National Academy of Sciences *117*, 10422-10428.
37. Formoso, K.K., Nesbitt, S.J., Pritchard, A.C., Stocker, M.R., and Parker, W.G. (2019). A long-necked tanystropheid from the Middle Triassic Moenkopi Formation (Anisian) provides insights into the ecology and biogeography of tanystropheids. Palaeontologia Electronica *22*, 1-15.
38. Wintrich, T., Jonas, R., Wilke, H.-J., Schmitz, L., and Sander, P.M. (2019). Neck mobility in the Jurassic plesiosaur *Cryptoclidus eurymerus*: finite element analysis as a new approach to understanding the cervical skeleton in fossil vertebrates. PeerJ *7*, e7658.
39. Chinsamy, A. (1993). Bone histology and growth trajectory of the prosauropod dinosaur *Massospondylus carinatus* Owen. Modern Geology *18*, 319-329.
40. Köhler, M., Marín-Moratalla, N., Jordana, X., and Aanes, R. (2012). Seasonal bone growth and physiology in endotherms shed light on dinosaur physiology. Nature *487*, 358.
41. Woodward, H.N., Horner, J.R., and Farlow, J.O. (2011). Osteohistological evidence for determinate growth in the American alligator. Journal of Herpetology *45*, 339-343.
42. Melstrom, K.M. (2017). The Relationship Between Diet and Tooth Complexity in Living Dentigerous Saurians. Journal of Morphology *278*, 500-522.
43. Rieppel, O., Mazin, J.-M., and Tchernov, E. (1997). Speciation along rifting continental margins: a new nothosaur from the Negev (Israel). Comptes Rendus de l'Académie des Sciences-Series IIA-Earth and Planetary Science *325*, 991-997.
44. Foffa, D., Young, M.T., Stubbs, T.L., Dexter, K.G., and Brusatte, S.L. (2018). The long-term ecology and evolution of marine reptiles in a Jurassic seaway. Nature ecology & evolution *2*, 1548-1555.
45. Rieppel, O. (2001). A new species of *Tanystropheus* (Reptilia: Protorosauria) from the Middle Triassic of Makhtesh Ramon, Israel. Neues Jahrbuch für Geologie und Paläontologie Abhandlungen *221*, 271-287.
46. Rieppel, O. (1985). Die Triasfauna der Tessiner Kalkalpen: XXV. Die Gattung *Saurichthys* (Pisces, Actinopterygii) aus der mittleren Trias des Monte San Giorgio, Kanton Tessin. Schweizerische Paläontologische Abhandlungen *108*, 1-81.
47. Rieppel, O. (1992). A new species of the genus *Saurichthys* (Pisces: Actinopterygii) from the Middle Triassic of Monte San Giorgio (Switzerland), with comments on the phylogenetic interrelationships of the genus. Palaeontographica. Abteilung A, Paläozoologie, Stratigraphie *221*, 63-94.
48. Bürgin, T. (1996). Diversity in the feeding apparatus of perleidid fishes (Actinopterygii) from the Middle Triassic of Monte San Giorgio (Switzerland). In Mesozoic Fishes – Systematics and Paleoecology, G. Arratia and G. Viohl, eds. (Munich: F. Pfeil).
49. Wild, R. (1987). An example of biological reasons for extinction: *Tanystropheus* (Reptilia, Squamata). Mémoires de la Société Géologique de France, n. s. *150*, 37-44.
50. Taylor, M.A. (1989). Neck and neck. Nature *341*, 668-689.
51. Cau, A., Beyrand, V., Voeten, D.F., Fernandez, V., Tafforeau, P., Stein, K., Barsbold, R., Tsogtbaatar, K., Currie, P.J., and Godefroit, P. (2017). Synchrotron scanning reveals amphibious ecomorphology in a new clade of bird-like dinosaurs. Nature *552*, 395-399.

52. Mirone, A., Brun, E., Gouillart, E., Tafforeau, P., and Kieffer, J. (2014). The PyHST2 hybrid distributed code for high speed tomographic reconstruction with iterative reconstruction and a priori knowledge capabilities. Nuclear Instruments and Methods in Physics Research Section B: Beam Interactions with Materials and Atoms *324*, 41-48.
53. Paganin, D., Mayo, S.C., Gureyev, T.E., Miller, P.R., and Wilkins, S.W. (2002). Simultaneous phase and amplitude extraction from a single defocused image of a homogeneous object. Journal of Microscopy *206*, 33-40.
54. Lyckegaard, A., Johnson, G., and Tafforeau, P. (2011). Correction of ring artifacts in X-ray tomographic images. International Journal of Tomography & Statistics *18*, 1-9.
55. Chinsamy, A., and Raath, M.A. (1992). Preparation of fossil bone for histological examination. Palaeontologia Africana *29*, 39-44.
56. Pritchard, A.C., Turner, A.H., Nesbitt, S.J., Irmis, R.B., and Smith, N.D. (2015). Late Triassic tanystropheids (Reptilia, Archosauromorpha) from Northern New Mexico (Petrified Forest Member, Chinle Formation) and the biogeography, functional morphology, and evolution of Tanystropheidae. Journal of Vertebrate Paleontology, e911186.
57. Nesbitt, S.J., Flynn, J.J., Pritchard, A.C., Parrish, J.M., Ranivoharimanana, L., and Wyss, A.R. (2015). Postcranial anatomy and relationships of *Azendohsaurus madagaskarensis*. Bulletin of the American Museum of Natural History *398*, 1-126.
58. Pritchard, A.C., and Nesbitt, S.J. (2017). A bird-like skull in a Triassic diapsid reptile increases heterogeneity of the morphological and phylogenetic radiation of Diapsida. Royal Society Open Science *4*.
59. Pritchard, A.C., Turner, A.H., Irmis, R.B., Nesbitt, S.J., and Smith, N.D. (2016). Extreme Modification of the Tetrapod Forelimb in a Triassic Diapsid Reptile. Current Biology *26*, 1-8.
60. Pritchard, A.C., Gauthier, J.A., Hanson, M., Bever, G.S., and Bhullar, B.-A.S. (2018). A tiny Triassic saurian from Connecticut and the early evolution of the diapsid feeding apparatus. Nature communications *9*, 1213.
61. Scheyer, T.M., Spiekman, S.N.F., Butler, R.J., Ezcurra, M.D., Sues, H.-D., and Jones, M.E.H. (2020). *Colobops*, a juvenile rhynchocephalian reptile (Lepidosauromorpha), not a diminutive archosauromorph with an unusually strong bite. Royal Society Open Science *7*, 1-14.
62. Benton, M.J., and Allen, J.L. (1997). *Boreopricea* from the Lower Triassic of Russia, and the relationships of the prolacertiform reptiles. Palaeontology *40*, 931-953.
63. Goloboff, P.A., and Catalano, S.A. (2016). TNT version 1.5, including a full implementation of phylogenetic morphometrics. Cladistics *32*, 221-238.

Figure 1.

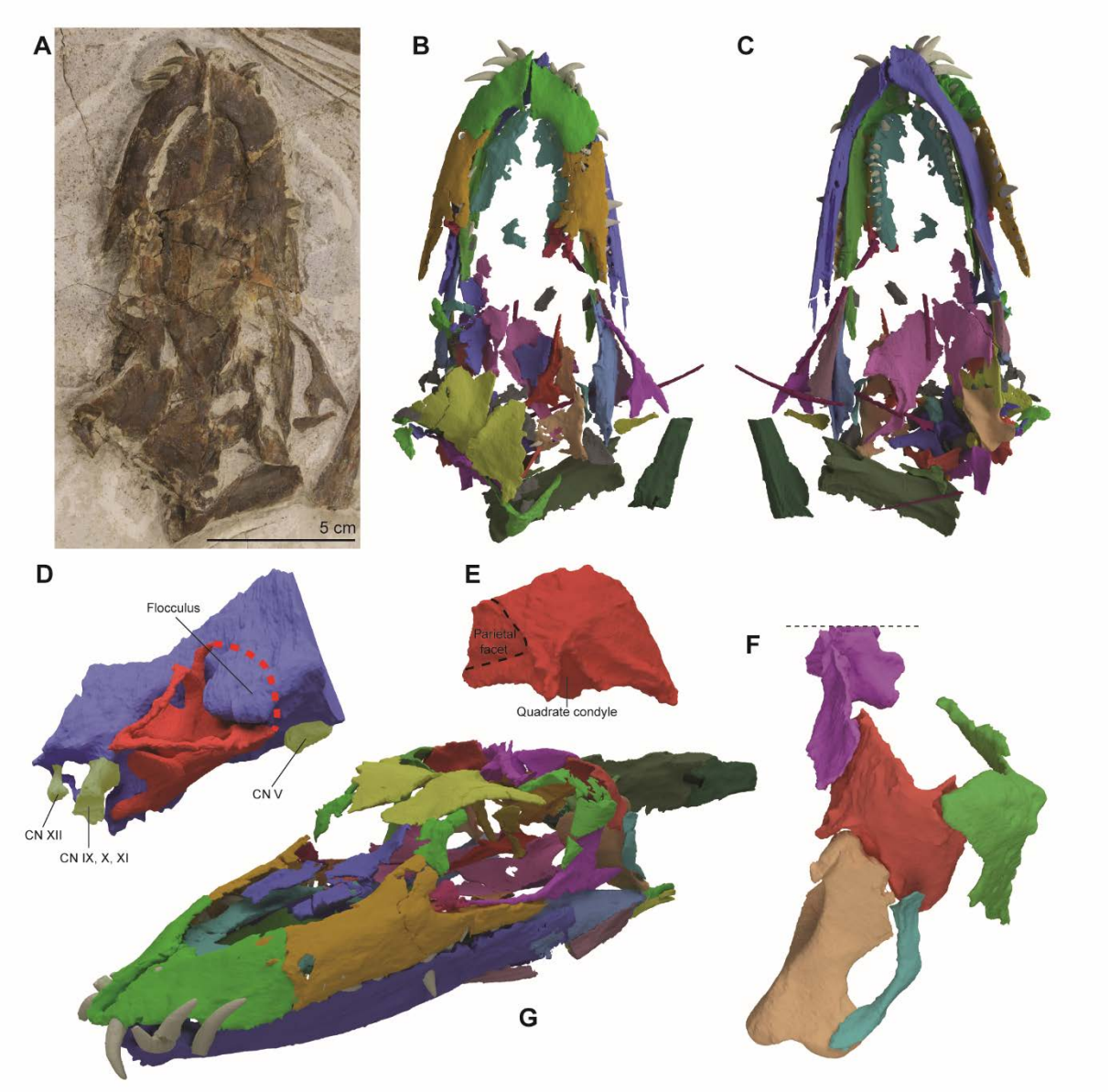
A
5 cm
B
C
D
Flocculus
CN V
CN XII
CN IX, X, XI
E
Parietal facet
Quadrate condyle
F
G

544 **Figure 2.**

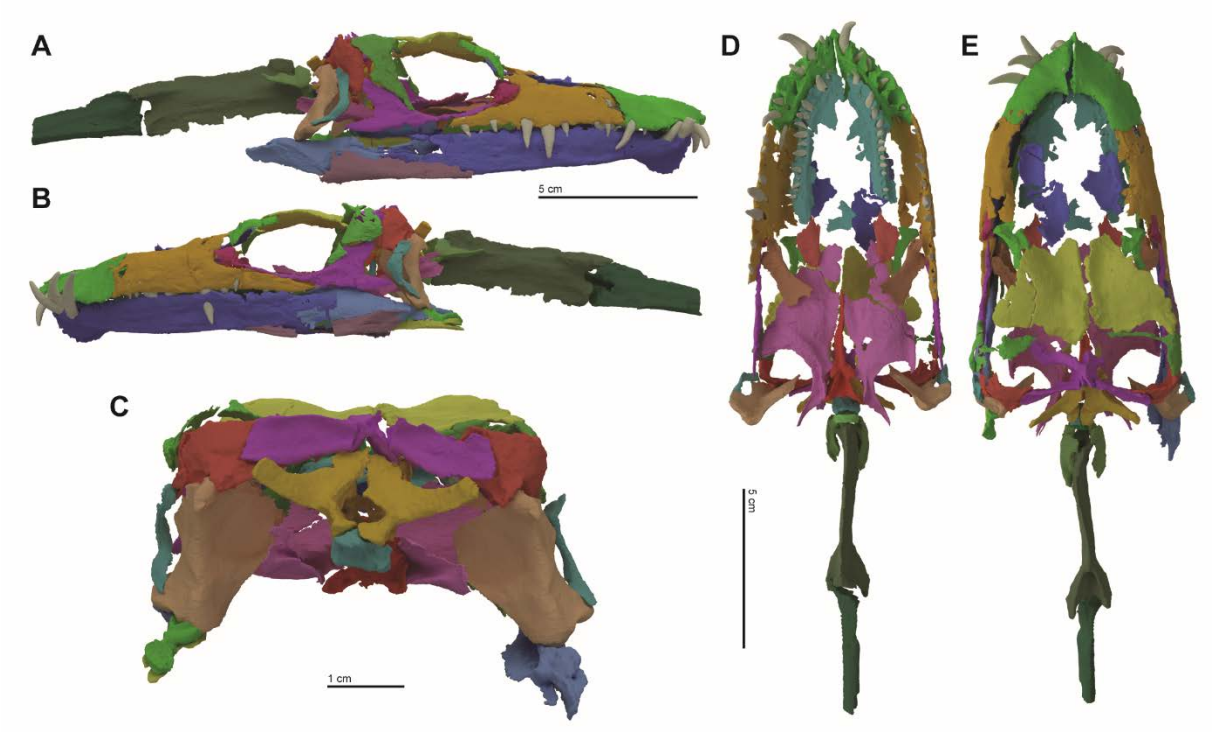

545

546

547 **Figure 3.**

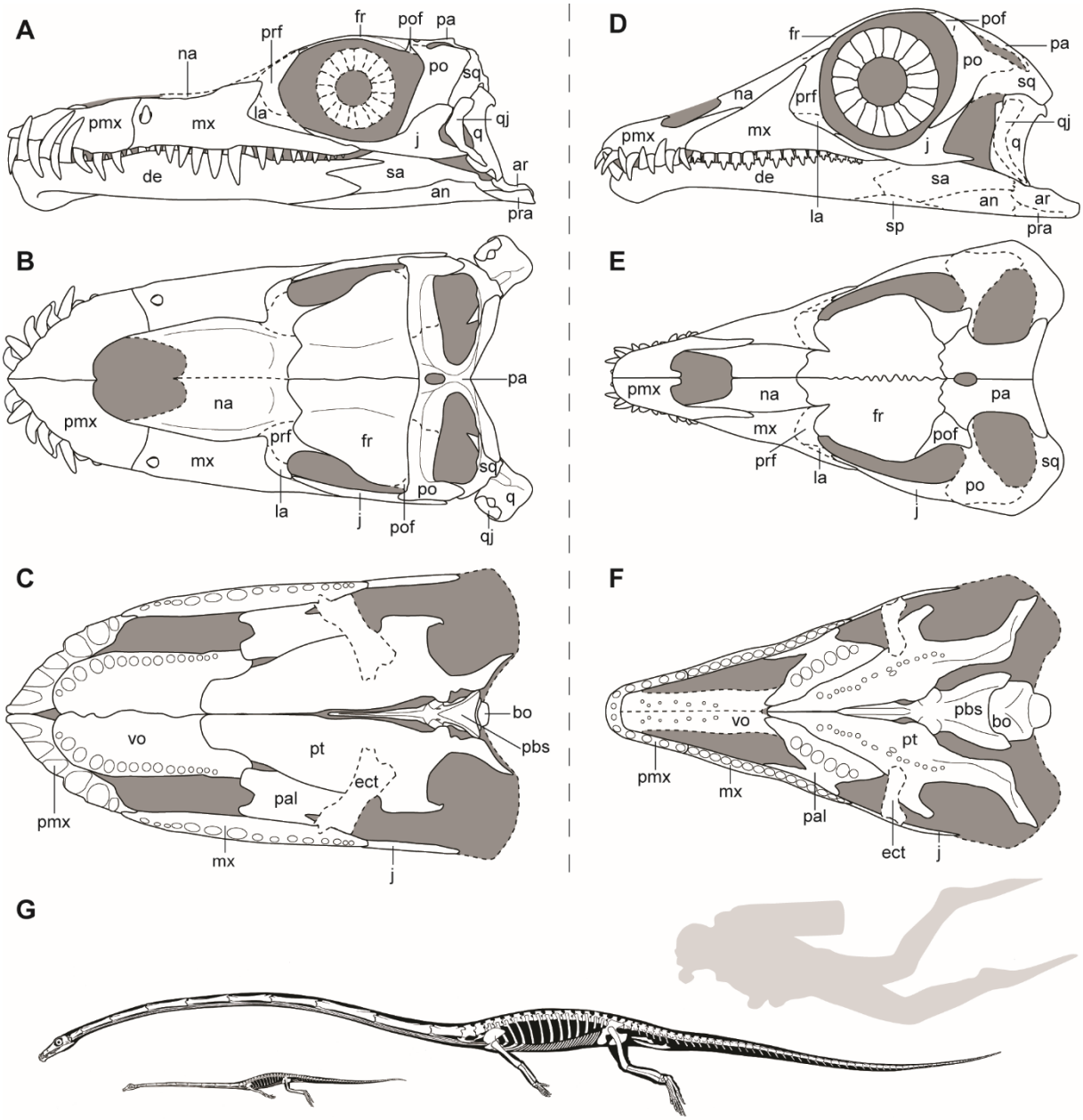

548

549

550 **Figure 4.**

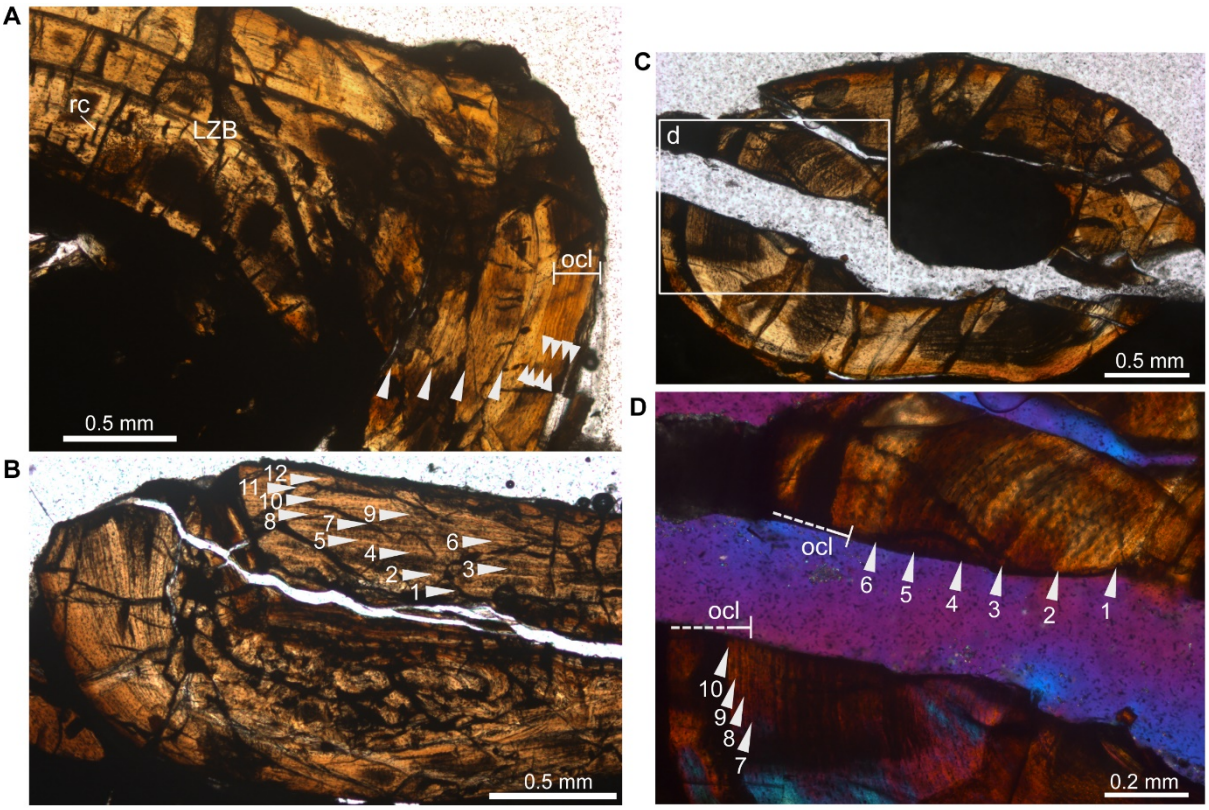

551

552 **Key Resources Table**

REAGENT or RESOURCE	SOURCE	IDENTIFIER
Biological Samples		
Tanystropheus hydroides (skull, mandibles, atlas-axis complex, and cervical vertebra 3)	This paper	PIMUZ T 2790
Tanystropheus longobardicus (femur thin-section)	This paper	PIMUZ T 1277
Tanystropheus longobardicus (zeugopodial element thin-section)	This paper	PIMUZ T 1277
Tanystropheus longobardicus (femur thin-section)	This paper	PIMUZ T 2484
Tanystropheus longobardicus (disarticulated skull)	This paper	PIMUZ T 2484
Tanystropheus hydroides (skull)	This paper	PIMUZ T 2819
Tanystropheus hydroides (disarticulated skull)	This paper	PIMUZ T 2787
Deposited Data		
SRµCT data of PIMUZ T 2790	This paper	https://www.paleo.esrf.fr.
The digital models of PIMUZ T 2790	This paper	https://www.paleo.esrf.fr.
Palaeohistological thin sections	This paper	Figure S3
Nexus file for phylogenetic analysis	This paper	Supplementary data file
Video files of digital models of PIMUZ T 2790	This paper	Supplementary data file
Software and Algorithms		
Mimics Research v19.0	https://biomedical.materialise.com/mimics	N/A
Blender 2.7	https://blender.org	N/A
TNT 1.5	[63]	N/A

553

554

Methods S1

Revision of *Tanystropheus longobardicus*

Systematic palaeontology

Diapsida Osborn, 1903 [S1]

Archosauromorpha von Huene, 1946 [S2]

Tanystropheidae Camp 1945 [S3]

Tanystropheus von Meyer, 1852 [S4]

Tanystropheus longobardicus Bassani, 1886 [S5]

Note to family-group name

Gervais (1858) has widely been cited as first mentioning the family-group Tanystropheidae. However, this text contains no reference to either Tanystropheidae or *Tanystropheus* [S6]. *Tanystropheus* remains are referred to as "Les Tanystrophes" in Gervais (1859), but this does not constitute a valid family-group name [S7]. Instead, Camp (1945) first published the family-group name Tanystrophaeidae, based on *Tanystrophaeus* (introduced by Cope, 1887 [S8]), which is an incorrect spelling of *Tanystropheus* von Meyer, 1852 [S3]. Therefore, the corrected name should be Tanystropheidae Camp, 1945 following article 35.4.1 of the ICZN.

Neotype

PIMUZ T 2791, a nearly complete semi-articulated specimen missing the posterior tail section.

Referred material

PIMUZ T 2779, PIMUZ T 2781, PIMUZ T 2795, PIMUZ T 2485, PIMUZ T 2482, PIMUZ T 2484, PIMUZ T 3901, PIMUZ T 1277, MSNM BES SC 265, MSNM BES SC 1018. A synonymy list is provided in ref. [S9] (as small morphotype *T. longobardicus*).

Locality

Monte San Giorgio on the border of Switzerland (canton Ticino) and Italy (Lombardy).

Horizon

Besano Formation, Anisian-Ladinian boundary; and Meride Limestone, Cassina beds, Ladinian; both Middle Triassic.

Emended diagnosis

Tanystropheus longobardicus is distinguished from other *Tanystropheus* species by the following combination of characters: Premaxilla with a pronounced postnarial process; tricuspid dentition on the maxilla and dentary; no dentary tooth piercing through a foramen in the maxilla; dorsal surface of the nasals is flattened; interdigitating suture between frontals; unfused parietals; dorsal head of quadrate without a conspicuous hook; elongate and narrow vomer bearing small teeth; palatine and

pterygoid tooth bearing; dentary lacking a ventral keel on its anterior end; maximum total body size of less than 2 metres.

***New insights into the cranial morphology of* T. longobardicus**

The cranial morphology of *T. longobardicus* was previously described in detail (at the time considered as the small morphotype or juvenile form of *T. longobardicus*) [S10, 11]. Our new findings for *T. hydroides* and a re-evaluation of the specimens of *T. longobardicus* allow for the reinterpretation of some aspects of the morphology of *T. longobardicus* that were previously misinterpreted due to the lack of three-dimensionally preserved specimens in this species (Figures 3D-F and S2D-E).

Tanystropheus longobardicus was previously reconstructed with an internarial bar formed by a long anteromedial process of the nasal [S10, 11]. As in *T. hydroides*, the nasals are generally poorly preserved, and the only complete nasals for *T. longobardicus* are known from the disarticulated specimen PIMUZ T 2484 (Figure S2D). By comparing the articulation surfaces of the nasals and frontals, it is revealed that the nasals are only able to connect to the frontals when the anterior process of the nasal is located at the anterolateral rather than the anteromedial side of the element (Figure S2D-E). Based on this interpretation, it becomes clear that like *T. hydroides*, *T. longobardicus* also lacked an internarial bar and consequently possessed confluent external nares (Figure 3D-E).

Similar to *T. hydroides*, the frontals of *T. longobardicus* are broad and they were interpreted to overhang the orbits laterally [S10]. However, based on the reinterpretation of the articulation between the nasals and frontals of *T. longobardicus*, it becomes clear that the prefrontal and possibly the lacrimal would have articulated with the anterolateral margin of the frontal. As such, the frontal would not have projected out over the orbit, but rather would have formed a wide dorsal skull roof surface between both orbits (Figure 3E). Therefore, as in *T. hydroides*, the orbits of *T. longobardicus* would have largely faced laterally.

The preservation of the squamosal and postorbital in PIMUZ T 2790 (Figure 1F) allows for several reinterpretations of these elements for *T. longobardicus* (Figure 3D-F). Based on elements identified as the squamosal in the neotype PIMUZ T 2791, in PIMUZ T 2484, and MSNM BES SC 265, the squamosal of *T. longobardicus* was previously reconstructed as being a thin 'boomerang-shaped' element that bears two elongate and curved processes and a much smaller third process [S10, 11]. This morphology stands in stark contrast to the morphology of the squamosal of *T. hydroides* but strongly corresponds to the morphology of its postorbital as they are confidently established here. These elements are therefore re-identified as postorbitals, and their morphology is in congruence with the correctly identified postorbital of *T. longobardicus* specimen MSNM BES SC 1018 [S10]. Similarly, the elements identified as the squamosals in the *T. hydroides* specimen PIMUZ T 2787 also represent postorbitals and the element identified as the postorbital in that specimen represents a squamosal [S11]. The morphology of the squamosal is poorly represented in any of the known specimens of *T. longobardicus*.

A small, curved quadratojugal oriented parallel to the shaft of the quadrate has been unequivocally identified here for *T. hydroides*. This element was previously considered to be absent in both the large and small morphotype of *T. longobardicus*. It is possible that this element was also present in the newly diagnosed *T. longobardicus*. However, it cannot be confidently identified among the specimens currently available [S10, 11].

Description of histological sections

The cross section of the femur of PIMUZ T 1277, a specimen of *Tanystropheus longobardicus*, exhibits lamellar-zonal compact bone (Figures 4A and S3A), as was previously also described for the genus [S12]. This structure is typical of a 'slow-growing' reptile and is found in many extant squamates and crocodylians [S13-17]. The outer cortex of the bone is only preserved along a small section and was elsewhere partially destroyed during acid preparation of the specimen. At least 12 lines of arrested growth (LAGs) are present, although their exact number could not be established. Eight of the LAGs are tightly bundled together near the outer margin of the bone to form an outer circumferential layer (OCL; also known as an external fundamental system or EFS), indicating that the growth of the animal had effectively ceased at the end of the life of this individual [S18]. The sampled zeugopodial element confirmed the high number of growth marks and the presence of an OCL/EFS (Figures 4C-D and S3B), whereas the femur of PIMUZ T 2484 shows LAGs throughout the cortex, but an OCL/EFS was not obvious (Figures 4B and S3C).

Phylogenetic analysis

The following characters were modified from Pritchard et al. 2018 [S19] (modifications indicated in **bold**):

6) Premaxilla, posterodorsal process, maxilla contact: (*0*) simple, straight suture; (*1*) margin/knob on the posterior margin of the posterodorsal process of the premaxilla fits into notch in the anterior surface of the maxilla; (*2*) anterior lamina of maxilla laps laterally over posterodorsal process of premaxilla**; (*3*) posterodorsal process of premaxilla laterally overlaps anterior lamina of maxilla.**

10) Maxilla, lateral surface near anteroposterior midpoint: (*0*) marked by subequal neurovascular foramina; (*1*) bears single neurovascular foramen that is anteroposteriorly longer than all others**; (*2*) no maxillary neurovascular foramina present**.

Phylogenetic implications

Our analysis recovered a monophyletic Tanystropheidae as one of the earliest diverging lineages within the archosaur stem-group Archosauromorpha, corresponding to ref. [S19] (Figure S4). Within Tanystropheidae, *Tanystropheus hydroides* and *Tanystropheus longobardicus* represent sister taxa. In contrast to ref. [S19], our results indicate that Tanystropheidae are more closely related to Archosauriformes than Allokotosauria. Tanystropheidae shares the following synapomorphies with rhynchosaurs, *Prolacerta broomi*, and Archosauriformes: distally bifurcating second sacral rib (131-1), coracoid lacking a tubercle (146-1), humerus with a low double distal condyle (156-1), absence of a medial centrale of the manus (158-0). Previously, allokotosaurs were considered to be closely related to Archosauriformes [S20]. Our results challenge this hypothesis and indicate that there is currently no clear consensus regarding the interrelationships of non-archosauriform archosauromorph clades.

As the best-known member of Tanystropheidae, which is one of the earliest and most stemward archosauromorph clades, *Tanystropheus* is crucial in understanding the origin of the modern

archosaur and lepidosaur lineages. Unfortunately, cranial material for other tanystropheid taxa is currently limited, except for *Macrocnemus* spp. [S21, 22]. Although they reveal a strong similarity in the morphology of the postcranial skeleton, the cranial morphology between *Tanystropheus* and *Macrocnemus* is remarkably different. This suggests that Tanystropheidae were considerably more ecomorphologically diverse than can currently be appreciated. Furthermore, the occurrence of a highly specialized taxon that adapted to exploit different food sources indicates the variability within stem-archosaurs and highlights their diversity during the Middle Triassic.

Supplemental References.

S1. Osborn, H.F. (1903). The reptilian subclasses Diapsida and Synapsida and the early history of the Diaptosauria. Memoirs of the American Museum of Natural History *1*, 449-519.

S2. Huene, F.R.v. (1946). Die grossen Stämme der Tetrapoden in den geologischen Zeiten. Biologisches Zentralblatt *65*, 268-275.

S3. Camp, C.L. (1945). *Prolacerta* and the protorosaurian reptiles. Part I and Part II. American Journal of Science *243*, 17-32, 84-101.

S4. Meyer, H.v. (1855). Die Saurier des Muschelkalkes mit Rücksicht auf die Saurier aus buntem Sandstein und Keuper. In Zur Fauna der Vorwelt, zweite Abtheilung, H. Keller, ed. (Frankfurt a.m.: Heinrich Keller).

S5. Bassani, F. (1886). Sui fossili e sull'eta degli schisti bituminosi triasici di Besano in Lombardia. Atti Società Italiana di scienze naturali *29*, 15-72.

S6. Gervais, P. (1858). Description de l'*Aphelosaurus latevensis*, saurien fossile des schistes Permiens de Lodeve. Annales de Sciences Naturelles *10*, 233-235.

S7. Gervais, P. (1859). Zoologie et paléontologie françaises: nouvelles recherches sur les animaux vertébrés dont on trouve les ossements enfouis dans le sol de la France et sur leur comparaison avec les espèces propres aux autres régions du globe, (A. Bertrand).

S8. Cope, E.D. (1887). A contribution to the history of the Vertebrata of the Trias of North America. Proceedings of the American Philosophical Society *24*, 209-228.

S9. Spiekman, S.N.F., and Scheyer, T.M. (2019). A taxonomic revision of the genus *Tanystropheus* (Archosauromorpha, Tanystropheidae). Palaeontologia Electronica *22*, 1-46.

S10. Nosotti, S. (2007). *Tanystropheus longobardicus* (Reptilia, Protorosauria): Re-interpretations of the anatomy based on new specimens from the Middle Triassic of Besano (Lombardy, northern Italy). Memorie della Società Italiana di Scienze Naturali e del Museo Civico di Storia Naturale di Milano *35*, 1-88.

S11. Wild, R. (1973). Die Triasfauna der Tessiner Kalkalpen XXII. *Tanystropheus longobardicus* (Bassani) (Neue Ergebnisse). Schweizerische Paläontologische Abhandlungen *95*, 1-182.

S12. Jaquier, V.P., and Scheyer, T.M. (2017). Bone Histology of the Middle Triassic Long-Necked Reptiles *Tanystropheus* and *Macrocnemus* (Archosauromorpha, Protorosauria). Journal of Vertebrate Paleontology.

S13. Woodward, H.N., Horner, J.R., and Farlow, J.O. (2011). Osteohistological evidence for determinate growth in the American alligator. Journal of Herpetology *45*, 339-343.

S14. Klein, N., Scheyer, T., and Tütken, T. (2009). Skeletochronology and isotopic analysis of a captive individual of *Alligator mississippiensis* Daudin, 1802. Fossil Record *12*, 121-131.

S15. Francillon-Vieillot, H., De Buffrénil, V., Castanet, J., Géraudie, J., Meunier, F., Sire, J., Zylberberg, L., and De Ricqlès, A. (1990). Microstructure and mineralization of vertebrate skeletal tissues. Skeletal biomineralization: patterns, processes and evolutionary trends *1*, 471-530.

S16. de Buffrénil, V., and Castanet, J. (2000). Age estimation by skeletochronology in the Nile monitor (*Varanus niloticus*), a highly exploited species. Journal of Herpetology, 414-424.

S17. Hugi, J., and Sánchez-Villagra, M.R. (2012). Life history and skeletal adaptations in the Galapagos marine iguana (*Amblyrhynchus cristatus*) as reconstructed with bone histological data—a comparative study of iguanines. Journal of Herpetology, 312-324.

S18. Ponton, F., Elżanowski, A., Castanet, J., Chinsamy, A., De Margerie, E., De Ricqlès, A., and Cubo, J. (2004). Variation of the outer circumferential layer in the limb bones of birds. Acta Ornithologica *39*, 137-140.

S19. Pritchard, A.C., Gauthier, J.A., Hanson, M., Bever, G.S., and Bhullar, B.-A.S. (2018). A tiny Triassic saurian from Connecticut and the early evolution of the diapsid feeding apparatus. Nature communications *9*, 1213.

S20. Nesbitt, S.J., Flynn, J.J., Pritchard, A.C., Parrish, J.M., Ranivoharimanana, L., and Wyss, A.R. (2015). Postcranial anatomy and relationships of *Azendohsaurus madagaskarensis*. Bulletin of the American Museum of Natural History *398*, 1-126.

S21. Jaquier, V.P., Fraser, N.C., Furrer, H., and Scheyer, T.M. (2017). Osteology of a New Specimen of *Macrocnemus* aff. *M. fuyuanensis* (Archosauromorpha, Protorosauria) from the Middle Triassic of Europe: Potential Implications for Species Recognition and Paleogeography of Tanystropheid Protorosaurs. Frontiers in Earth Science *5*.

S22. Scheyer, T.M., Wang, W., Li, C., Miedema, F., and Spiekman, S.N.F. (2020). Osteological re-description of *Macrocnemus fuyuanensis* (Archosauromorpha, Tanystropheidae) from the Middle Triassic of China. Vertebrata PalAsiatica.

S23. Pritchard, A.C., Gauthier, J.A., Hanson, M., Bever, G.S., and Bhullar, B.-A.S. (2018). A tiny Triassic saurian from Connecticut and the early evolution of the diapsid feeding apparatus. Nature communications *9*, 1213.

Supplemental data

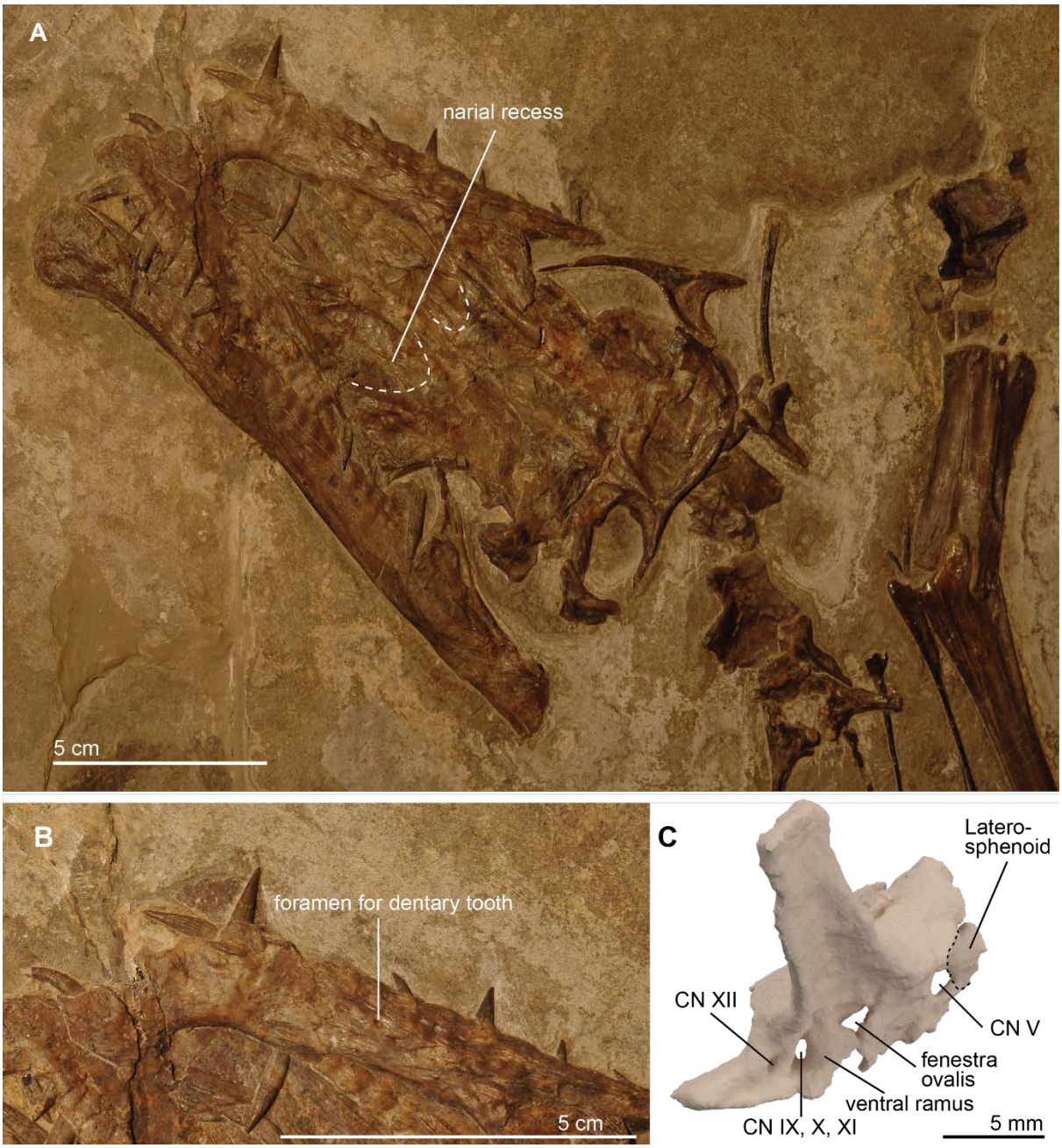

Figure S1. The skull and braincase of *Tanystropheus hydroides* sp. nov. Related to Figure 3. (A) Complete skull of PIMUZ T 2819. (B) Close-up of the right anterior snout region of PIMUZ T 2819 revealing the opening for a dentary tooth in the right maxilla. (C) Digital rendering of the right partial braincase of PIMUZ T 2790 in lateral view.

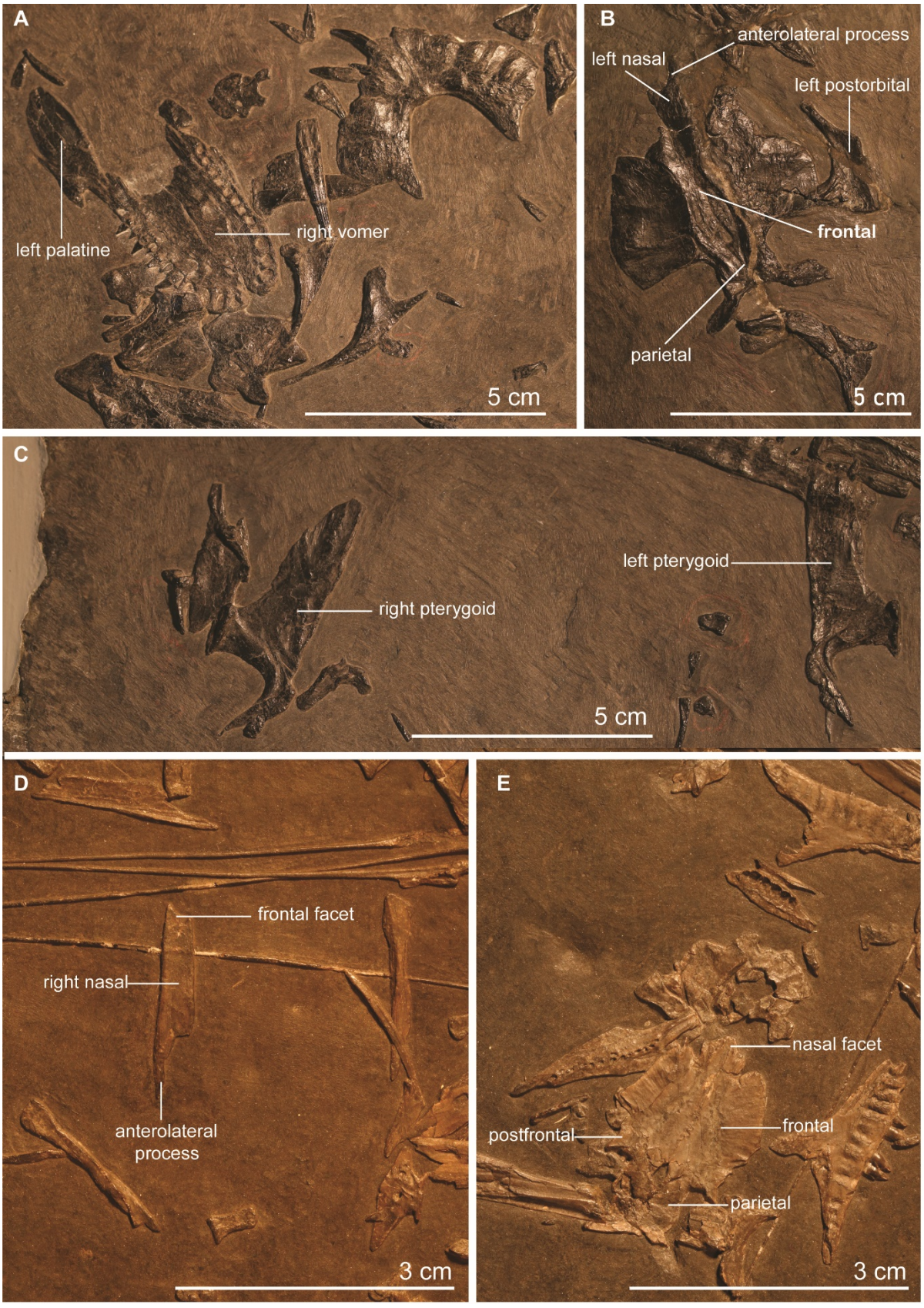

747

748 **Figure S2. Specific anatomical details of additional *Tanystropheus* specimens. Related to Figure 3.**
749 (A-C) *Tanystropheus hydroides* sp. nov. PIMUZ T 2787. (D-E) *Tanystropheus longobardicus* PIMUZ T
750 2484.

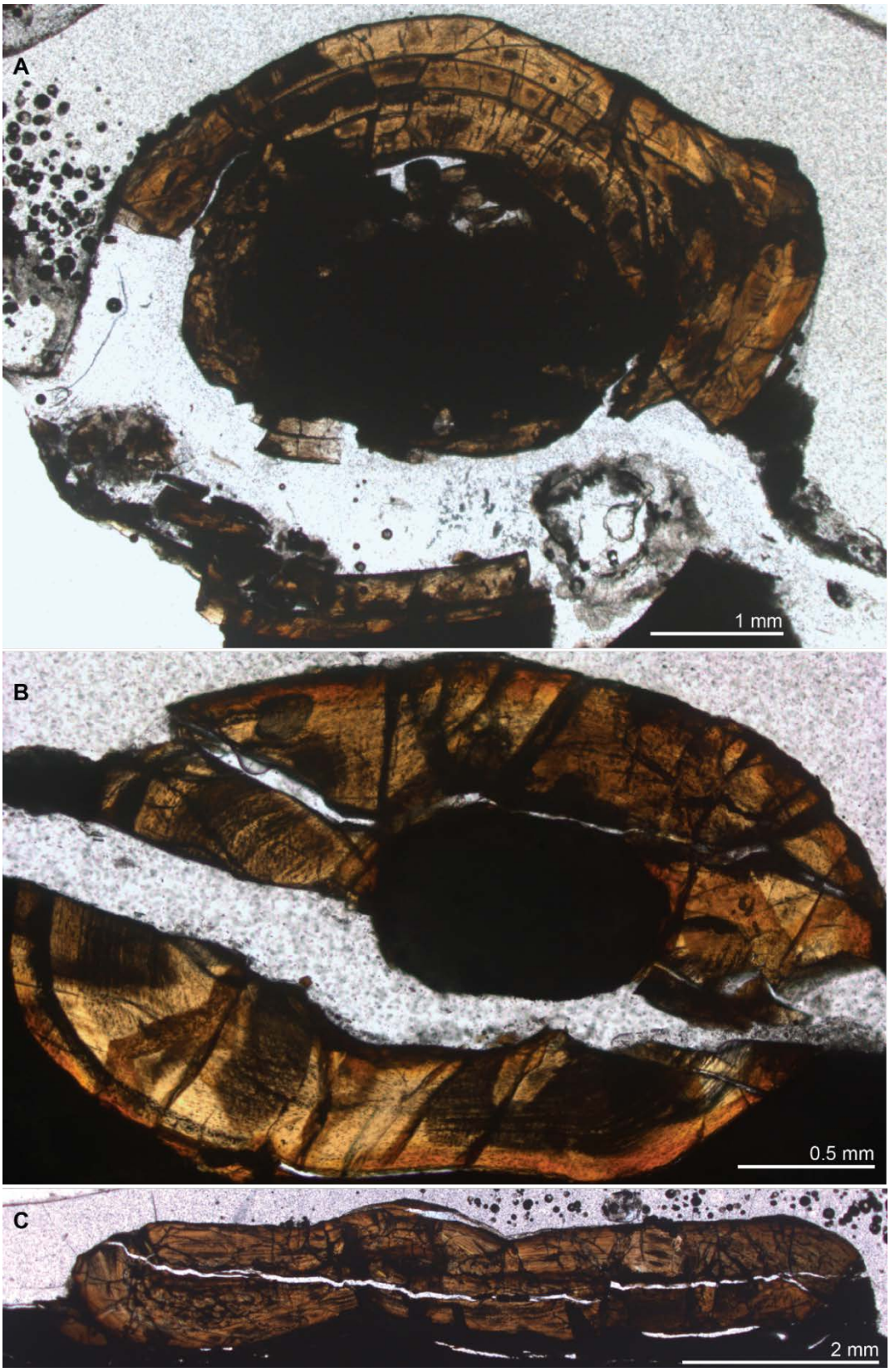

Figure S3. Overview of the studied histological sections in normal transmitted light. Related to Figure 4. (A) Mid-shaft section of the femur of PIMUZ T 1277, (B) mid-shaft section of the zeugopodial element (radius or ulna) of PIMUZ T 1277, (C) mid-shaft section of the femur of PIMUZ T 2484.

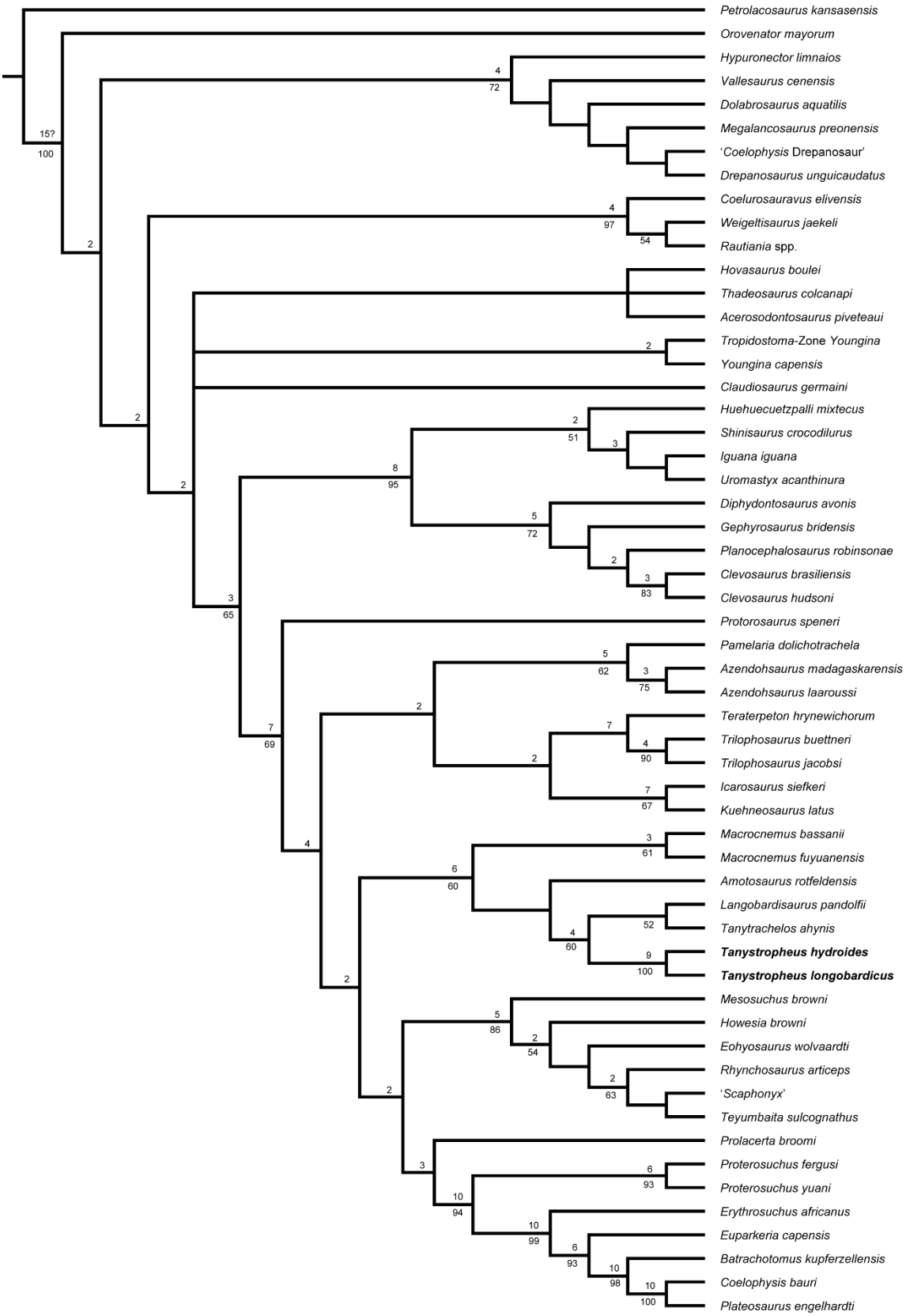

Figure S4. Complete strict consensus tree of the three most parsimonious trees (1125 steps; CI=0.324; RI=0.648). Related to STAR Methods. Bremer values above 1 are indicated above each node and Bootstrap frequencies above 50% are shown below each node.

Elements	Colour	Preserved element
Premaxilla	Green	Both
Maxilla	Orange	Both
Nasal	Blue	Both (partially)
Lacrimal	Purple	Left (mirrored for right)
Prefrontal	Green	Left (mirrored for right)
Frontal	Yellow	Both
Parietal	Purple	Single element
Postfrontal	n/a	Absent
Postorbital	Green	Both
Jugal	Purple	Right (partially reconstructed, mirrored for left)
Squamosal	Red	Both
Quadrate	Tan	Left (mirrored for right)
Quadratojugal	Light blue	Both
Vomer	Light blue	Both (partially)
Palatine	Red	Left (partially, mirrored for right)
Ectopterygoid	Tan	Right (mirrored for left)
Pterygoid	Pink	Both (partially)
Epipterygoid	Yellow	Both
Basioccipital	Light blue	Single element
Parabasisphenoid	Red	Single element
Exoccipital, opisthotic, supraoccipital, prootic, laterosphenoid (fused)	Orange	Both
Dentary	Blue	Both
Splenial	Green	Both
Angular	Pink	Both
Surangular	Light blue	Both (only isolated left)
Prearticular	Yellow	Both (only isolated left)
Articular	Green	Both (only isolated left)
Teeth	Grey	Various both sides

Table S1. An overview of the bones of the digitally reconstructed model of *Tanystropheus hydroides* sp. nov. PIMUZ T 2790. Related to Figures 1 and 2.